

Reversibility Violation in the Hybrid Monte Carlo Algorithm

Carsten Urbach¹

¹*HISKP (Theory) and BCTP, University of Bonn, Bonn, Germany*

We investigate reversibility violations in the Hybrid Monte Carlo algorithm. Those violations are inevitable when computers with finite numerical precision are being used. In $SU(2)$ gauge theory, we study the dependence of observables on the size of the reversibility violations. While we cannot find any statistically significant deviation in observables related to the simulated physical model, algorithmic specific observables signal an upper bound for reversibility violations below which simulations appear unproblematic. This empirically derived condition is independent of problem size and parameter values, at least in the range of parameters studied here.

I. INTRODUCTION

The Hybrid Monte Carlo (HMC) algorithm [1] is an exact accept/reject Markov chain Monte Carlo algorithm. It allows one to perform global updates combined with large acceptance rates. This property makes the HMC in its variants [2–4] and with its improvements [5–8] the workhorse for lattice Quantum Chromodynamics (QCD) simulations with dynamical fermions.

The HMC is composed of a molecular dynamics (MD) update and a Metropolis accept/reject step. During the MD update, Hamilton’s equations of motion (EOM) are integrated, in practice numerically. The accept/reject step corrects for finite integration step errors and renders the HMC exact. However, the proof of exactness requires the numerical integration scheme to be reversible and integration measure conserving. Numerical integration schemes conserving the integration measure are so-called symplectic integration schemes. A sub-set of these is also reversible, with the *leapfrog* integration scheme as the most well-known example.

Any practical realisation of such integration schemes suffers from round-off errors due to finite precision available on computers. In fact, it has been known since a long time that reversibility is violated in HMC simulations of lattice QCD [9–11]. Even further, the underlying equations of motion are chaotic in nature. Thus, any small round-off error will magnify exponentially during the integration. A corresponding positive Lyapunov exponent can be determined. Even though one may argue that these reversibility violations are a property of the algorithm, and not of the simulated system, it was conjectured [9] that this Lyapunov exponent obeys a continuum limit approached in a certain functional form with the coupling constant of the theory.

However, this hypothesis has never been finally verified or falsified. And, more importantly for practical simulations, to the knowledge of the author it has never been checked whether or not reversibility violations have any impact on observables. Analytic predictions are difficult here, because from a principle point of view the proof of exactness is no longer applicable once reversibility violations are present.

In this paper we are going to present an investigation of this issue in SU(2) gauge theory as a model. SU(2) gauge theory shares many properties with QCD, most importantly asymptotic freedom and confinement, but it requires much less computer resources than SU(3), not to speak about the inclusion of dynamical fermions. Therefore, we are able to study volume and lattice spacing dependencies.

This allows us to derive an empirical condition for how large reversibility violations appear tolerable in SU(2) gauge theory. It remains to be seen how this condition applies in case of QCD with SU(3) gauge fields and dynamical fermions.

In this paper we first describe the HMC algorithm followed by a description of SU(2) lattice gauge theory. Next we present results and finish with a discussion and summary. Most of the data tables can be found in the appendix.

II. THE HYBRID MONTE CARLO ALGORITHM

Assume we are after sampling field variables $\phi = \{\phi_x\}$, with x being a multi-index not further specified at this level, from a distribution

$$\phi \sim e^{-\mathcal{S}(\phi)}. \quad (1)$$

We call $\mathcal{S} \in \mathbb{R}$ the action, which is bounded from below. For the HMC one introduces auxiliary variables $\pi = \{\pi_x\}$ as conjugate momenta to the field variables ϕ and an artificial Hamiltonian

$$\mathcal{H}[\pi, \phi] = \frac{1}{2}\pi^2 + \mathcal{S}(\phi). \quad (2)$$

\mathcal{H} is conserved under Hamilton's equation of motion (EOM). Defining $z = (\pi, \phi)$, these EOMs may be written in the form

$$\dot{z} = \mathbb{J} \cdot \frac{\partial \mathcal{H}[z]}{\partial z}, \quad \mathbb{J} = \begin{pmatrix} 0 & -\mathbf{1} \\ \mathbf{1} & 0 \end{pmatrix}, \quad (3)$$

with $\mathbf{1}$ being unit matrices with dimension of x . In this form the symplectic structure of the EOMs becomes apparent. The dot notation represents time derivatives in an artificial HMC time τ . The HMC evolution starting from ϕ to ϕ' is then defined as follows:

1. Generate momenta π from a standard normal distribution.
2. Evolve $z \equiv z(0)$ in HMC time using Eq. 3 for a trajectory of length τ to arrive at $z(\tau)$. We denote this time evolution with $\mathcal{T}_{\mathcal{I}}(\tau)$ for integrator \mathcal{I} , such that

$$z(\tau) = \mathcal{T}_{\mathcal{I}}(\tau) z(0). \quad (4)$$

3. Compute

$$\Delta\mathcal{H} = \mathcal{H}[z(\tau)] - \mathcal{H}[z(0)]. \quad (5)$$

4. Accept $z(\tau)$ with probability

$$P_{\text{acc}} = \min\{1, \exp(-\Delta\mathcal{H})\}. \quad (6)$$

If accepted set $\phi' = \phi(\tau)$, else $\phi' = \phi(0)$.

5. restart at 1. with $\phi = \phi'$.

Reversibility of an integration scheme \mathcal{I} can now be written as

$$\mathcal{T}_{\mathcal{I}}(-\tau) \mathcal{T}_{\mathcal{I}}(\tau) z(0) = \mathcal{T}_{\mathcal{I}}(\tau) \mathcal{T}_{\mathcal{I}}(-\tau) z(0) = z(0). \quad (7)$$

For the integration measure to be conserved the Jacobi determinant of $\mathcal{T}_{\mathcal{I}}$ must be one. This is always the case if $\mathcal{T}_{\mathcal{I}}$ is symplectic. For an elementary and nicely accessible proof see Ref. [12].

In practice, the integration is performed with finite precision ϵ . Hence,

$$\mathcal{T}_{\mathcal{I}}^{\epsilon}(-\tau) \mathcal{T}_{\mathcal{I}}^{\epsilon}(\tau) z(0) = z(0) + \delta z(\epsilon). \quad (8)$$

In order to measure reversibility violations in an actual simulation one defines

$$\delta\Delta\mathcal{H} = \mathcal{H}[\mathcal{T}_{\mathcal{I}}^{\epsilon}(-\tau) \mathcal{T}_{\mathcal{I}}^{\epsilon}(\tau) z] - \mathcal{H}[z]. \quad (9)$$

A well known and very useful property of the HMC algorithm is

$$\langle \exp(-\Delta\mathcal{H}) \rangle = 1, \quad (10)$$

which follows analytically from the measure being conserved. Using this and the convexity of the exponential function it follows

$$\exp(-\langle \Delta\mathcal{H} \rangle) \leq 1 \quad \Rightarrow \quad \langle \Delta\mathcal{H} \rangle \geq 0. \quad (11)$$

Here, $\langle \cdot \rangle$ denotes the ensemble average over all generated z . We note in passing that symplecticity of the integration scheme implies the existence of a so-called shadow Hamiltonian which is exactly conserved under time evolution \mathcal{T} (see e.g. Ref. [13]).

Reversible integration schemes can be constructed to any order n in the discretisation error $\delta\tau^n$. The leapfrog (LF) is a second order integration scheme reading

$$\mathcal{T}_{\text{LF}}(\delta\tau) z(0) = \begin{cases} \phi(\delta\tau) = \phi(0) + \delta\tau \pi(\delta\tau/2) \\ \pi(\delta\tau) = \pi(\delta\tau/2) - \frac{\delta\tau}{2} \frac{\partial \mathcal{S}[\phi(\delta\tau)]}{\partial \phi(\delta\tau)} \end{cases}, \quad (12)$$

with

$$\pi(\delta\tau/2) = \pi(0) - \frac{\delta\tau}{2} \frac{\partial \mathcal{S}[\phi(0)]}{\partial \phi(0)}.$$

It represents a semi-implicit integration scheme and is symmetric around $\delta\tau/2$. In addition to the LF integration scheme we will use a fourth order integration scheme which we will conventionally denote as OMF4. Its details can be found in Ref. [14].

III. THE TOY MODEL: SU(2) GAUGE THEORY

We are going to work on a discrete and finite space-time lattice

$$V^\Lambda = (L_s/a)^3 \times L_t/a \equiv L^3 \times T \quad (13)$$

with a lattice spacing denoted as a and periodic boundary conditions. Hence, the possible set of coordinates is given as

$$\Lambda = \{x = (x_0, x_1, x_2, x_3) : x_0 = 0, \dots, T-1, x_{1,2,3} = 0, \dots, L-1\}. \quad (14)$$

We introduce so-called link variables $U_\mu(x) \in \text{SU}(2)$ connecting points x and $x + a\hat{\mu}$, where $\hat{\mu}$ is the unit vector in direction $\mu \in 0, 1, 2, 3$. For the discretised action we are going to use the Wilson plaquette gauge action reading

$$\mathcal{S}[U] = \frac{\beta}{2} a^4 \sum_{x \in \Lambda} \sum_{\mu < \nu} \text{Re Tr} [\mathbf{1}_2 - U_{\mu\nu}(x)] \quad (15)$$

with plaquette variables

$$U_{\mu\nu}(x) = U_\mu(x) U_\nu(x + a\hat{\mu}) U_\mu^\dagger(x + a\hat{\nu}) U_\nu^\dagger(x). \quad (16)$$

$\beta = 4/g_0^2$ is the inverse squared gauge coupling and g_0 the gauge coupling.

For the actual implementation it is used that any $U \in \text{SU}(2)$ can be written as

$$U = \begin{pmatrix} a & b \\ -b^* & a^* \end{pmatrix} \quad \text{with} \quad aa^* + bb^* = 1, \quad a, b \in \mathbb{C}, \quad (17)$$

which is a consequence of $\text{SU}(2)$ being homeomorphic to S^3 . Using Pauli matrices $\vec{\sigma}$, we may also write

$$U = x_0 \mathbf{1}_2 + i \vec{x} \vec{\sigma} \quad (18)$$

with $(x_0, \vec{x}) \in S^3$. This allows one to identify

$$x_0 = \text{Re}(a), \quad x_1 = \text{Im}(b), \quad x_2 = \text{Re}(b), \quad x_3 = \text{Im}(a). \quad (19)$$

The trace of an $\text{SU}(2)$ matrix is directly given by

$$\text{Tr } U = \text{Tr } U^\dagger = 2 \text{Re}(a). \quad (20)$$

The representation Eq. 18 is efficiently used in a numerical implementation, since only four real numbers need to be stored. One could reduce to only three real numbers, if $\det(U) = 1$ was used as well.

Using the Pauli matrices we can now introduce the derivative of a function $f(U), U \in \text{SU}(2)$ as follows

$$D_j f(U) = \left. \frac{\partial}{\partial \alpha} f(e^{i\alpha \sigma_j} U) \right|_{\alpha=0}, \quad j = 1, 2, 3. \quad (21)$$

This motivates to introduce the momenta conjugate to the $U_\mu(x)$ as $p_\mu^j(x) \in \mathbb{R}, j = 1, 2, 3$. The elementary update steps then read as follows

$$\begin{aligned} p_\mu^j(x)(\tau + \Delta\tau) &= p_\mu^j(x)(\tau) + \Delta\tau D_j \mathcal{S}, \quad j = 1, 2, 3, \\ U_\mu(x)(\tau + \Delta\tau) &= \exp \left[i\Delta\tau \sum_j p_\mu^j(x)(\tau + \Delta\tau/2) \sigma_j \right] U_\mu(x)(\tau). \end{aligned} \quad (22)$$

In order to study the response of the algorithm to increasing reversibility violations, we deliberately round on the right hand sides of Eqs. 22 to d significant decimal digits. To be precise, we replace Eqs. 22 by

$$\begin{aligned} p_\mu^j(x)(\tau + \Delta\tau) &= p_\mu^j(x)(\tau) + \Delta\tau [D_j \mathcal{S}]_d, \quad j = 1, 2, 3, \\ U_\mu(x)(\tau + \Delta\tau) &= \exp \left[i\Delta\tau \sum_j p_\mu^j(x)(\tau + \Delta\tau/2) \sigma_j \right] [U_\mu(x)(\tau)]_d. \end{aligned} \quad (23)$$

Eqs. 22 guarantee the U -fields to stay in $SU(2)$. However, with finite precision arithmetics this is only true up to rounding errors. Hence, we apply at the end of each MD evolution a projection to $SU(2)$ $P_{SU(2)}$. This is in particular important when $d < 16$. This projection step is applied before the accept/reject step, thus, $P_{SU(2)}$ will affect reversibility and measure conservation at the same level as before. All runs with $d < 16$ have been started from a well equilibrated (~ 5000 trajectories) configuration of a run without rounding.

If not specified otherwise, the trajectory length is always chosen to be $\tau = 1$. This holds for all β -values and volumes. As random number generator we use the Mersenne Twister algorithm [15] implemented in the C++ standard library. The $SU(2)$ simulation code is publicly available [16] and so is the analysis code [17].

A. Observables

During the run of the HMC we will measure observables on each trajectory. These are first of all the plaquette expectation value reading

$$\langle P \rangle = \frac{1}{6L^3T} \langle \sum_{x \in \Lambda} \sum_{\mu < \nu} \text{Tr} U_{\mu\nu}(x) \rangle. \quad (24)$$

The plaquette expectation value is one of the observables measurable with very high statistical accuracy and hence a good candidate for possible deviations. In addition to the plaquette itself, we also measure its integrated autocorrelation time $\tau_{\text{int}}(\langle P \rangle)$ using the methods described in Ref. [18].

Next, we measure of course $\Delta\mathcal{H}$ for each trajectory, which gives access to $\langle \Delta\mathcal{H} \rangle$ and $\langle \exp(-\Delta\mathcal{H}) \rangle$. The latter two are important to check whether Eq. 10 and Eq. 11 are fulfilled. It turns out that $\Delta\mathcal{H}$ shows no autocorrelation, as one would expect. Another quantity we measure for each trajectory is acceptance. From this we quantify the acceptance rate P_{acc} in percent.

More observables are measured only with a frequency of 100 trajectories. First of all, we measure $\delta\Delta\mathcal{H}$ by integrating backward in time. It turns out that $\delta\Delta\mathcal{H}$ is to a good approximation Gaussian distributed with mean zero and standard deviation $\text{sd}(\delta\Delta\mathcal{H})$, the latter of which depends directly on the number of significant digits used in the force calculation. Hence, $\text{sd}(\delta\Delta\mathcal{H})$ will be used as a measure for reversibility violations.

The plaquette represents the smallest closed Wilson loop which can be built on the lattice. As additional observables we consider planar Wilson loops of extension $t \times r$

$$C(t, r) = \frac{1}{3L^3T} \langle \sum_{x \in \Lambda} \sum_{\mu \neq 0} \text{Tr} U_{\mu}^{t,r}(x) \rangle. \quad (25)$$

β	t_0/a^2	s_0/a	N_{meas}
2.3	1.737(06)	1.318(2)	131
2.4	2.790(23)	1.670(7)	112
2.5	5.038(36)	2.245(8)	130

TABLE I: Gradient flow scales t_0 and $s_0 = \sqrt{t_0}$ for the β -values in lattice units for the β -values used in this study. We also give the number of well separated configurations N_{meas} we measured the scales on.

Here we denote the planar Wilson loop in spatial direction μ and with time extent t and spatial extent r by $U_\mu^{t,r}$. $C(t, r)$ decays at fixed r exponentially at large t like

$$C(t, r) \propto \exp(-V(r)t) \quad (26)$$

with $V(r)$ the so-called static quark potential at spatial distance r .

B. Lattice Scales

SU(2) gauge theory has been studied in the literature over many decades using lattice techniques, starting with the famous paper by Creutz [19] from 1980. Hence, scaling variables have been determined, see for instance Refs. [20–22]. Still, here we rely on the gradient flow [23], recently studied for SU(2) Yang-Mills theory in Ref. [24].

We follow the notation and the definitions of Ref. [23] and use the symmetric definition of the energy density E_{sym} . But since we work in SU(2), we use the following defining equation for the scale t_0

$$t^2 \langle E_{\text{sym}}(t) \rangle|_{t=t_0} = 0.1 \quad (27)$$

where t is the so-called flow time. Note that we chose 0.1 instead of original SU(3) value 0.3 in Eq. 27 following the reasoning in Ref. [25]. In addition we define the length scale s_0 via

$$s_0 = \sqrt{t_0}. \quad (28)$$

The choice of β -values used in this paper are motivated by the requirement to be in the scaling region. The values for t_0/a^2 and s_0/a we have determined for these β -values are compiled in Table I. The precision of the scales is not central to the results of this study, thus, we did not spend too many resources to obtain very precise results. The configurations used for determining t_0 were separated by at least 500 HMC trajectories and, hence, free of autocorrelation. For more details see the appendix.

Int	d	N_{traj}	$\langle P \rangle$	$\tau_{\text{int}}(P)$	$\langle \exp(-\Delta H) \rangle$	$\langle \Delta H \rangle$	$\text{sd}(\delta\Delta H)$	ρ	P_{acc}
LF	–	130000	0.60225(1)	6.3(2)	1.0001(18)	0.2008(17)	$2.0 \cdot 10^{-10}$	–0.02	75
LF	5	100737	0.60226(1)	5.9(2)	0.9991(21)	0.2048(20)	0.08087973	0.09	75
LF	4	98285	0.60226(1)	8.2(4)	0.9905(50)	0.6481(38)	0.7943932	0.42	57
OMF4	–	530000	0.602264(3)	5.8(1)	1.00026(45)	0.05312(44)	$1.5 \cdot 10^{-10}$	0	87
OMF4	6	420000	0.602266(3)	5.8(1)	1.00044(51)	0.05295(49)	0.005266247	0.01	87
OMF4	5	520000	0.602266(3)	5.8(1)	0.99903(46)	0.05541(45)	0.05406281	0.08	87
OMF4	4	480000	0.602266(3)	6.6(1)	0.99343(89)	0.16643(83)	0.528	0.46	77
OMF4	3	40000	0.6023(1)	251(71)	0.174(45)	11.337(30)	5.238426	0.59	2

TABLE II: Results at $\beta = 2.3$ and $L = 16$, $T = 32$. This can be compared to a Metropolis algorithm with $\langle P \rangle = 0.602266(6)$.

The ratios of our s_0 -values, given in Table I, can be compared to the results presented in Ref. [24]. Only roughly, because in Ref. [24] scales have been determined for $\beta = 2.3$, $\beta = 2.43$ and $\beta = 2.51$. Still, the agreement is reasonable.

IV. RESULTS

The statistical analysis of the Markov chains is performed using the so-called Γ -method described in Ref. [18]. In this way we include autocorrelation effects in the estimate of the standard error by estimating the integrated autocorrelation time τ_{int} of the observable in question. This analysis is double checked using a blocked bootstrap procedure, for which we find consistent results.

A. Results for $\beta = 2.3$

At the coarsest lattice spacing corresponding to $\beta = 2.3$ we have performed runs for three different spatial volumes $L = 12, 16, 20$ and a variety of significant digits d . We also compared the LF with the OMF4 integration scheme.

The runs and results for the observables $\langle P \rangle$, $\Delta\mathcal{H}$ related and $\delta\Delta\mathcal{H}$ are compiled for the different integration schemes and different d -values in Table II, Table III and Table IV. For better readability we have moved most of the tables to the appendix, apart from Table II. We quote ‘–’ for d if we run in double precision and perform no rounding. It roughly corresponds to $d = 16$.

For $L = 16$ we have carried out a comparison to a Metropolis algorithm, which yielded $\langle P \rangle = 0.602266(6)$ agreeing perfectly within statistical errors with the double precision HMC run, either

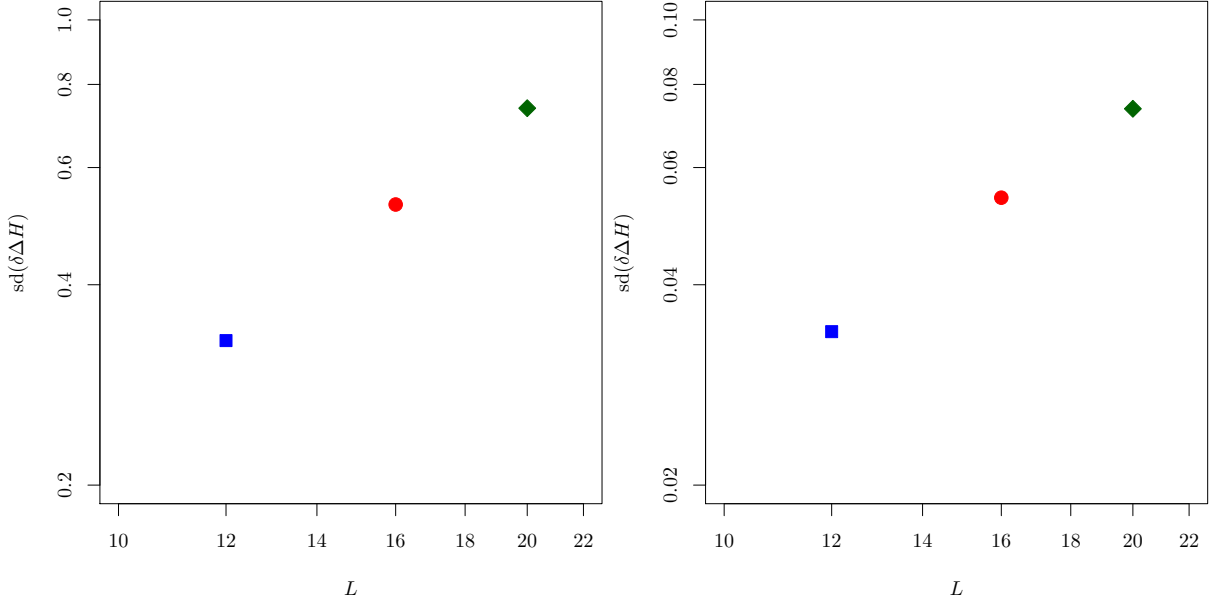


FIG. 1: $\text{sd}(\delta\Delta\mathcal{H})$ as a function of L in a double logarithmic plot for $\beta = 2.3$ and $L = 12, 16, 20$ with the OMF4 integration scheme. Left: $d = 4$. Right: $d = 5$. Note the factor 10 difference in the scale of the y -axes.

with LF or OMF4 integration scheme.

The values of d have been chosen as follows: we first determined the value of d where the HMC becomes instable. For $L = 16$ and $L = 12$ this was the case for $d = 3$, see Table II and Table III, respectively. This instability manifests itself in a significant increase in $\langle\Delta\mathcal{H}\rangle$ compared to the run without rounding, leading also to large drop in P_{acc} . These runs are clearly not reliable anymore, but also clearly identifiable as not reliable. That the plaquette expectation value is still roughly in line comes from the combination of low acceptance rate with an equilibrated initial gauge configuration.

Looking at the d dependence of $\text{sd}(\delta\Delta\mathcal{H})$, we find to a good approximation

$$\log_{10}(\text{sd}(\delta\Delta\mathcal{H})) = c_d(L, \mathcal{I}) d. \quad (29)$$

Therefore, we will replace d by $\text{sd}(\delta\Delta\mathcal{H})$ as a measure of reversibility violation. The coefficient c_d depends on the volume and the details of the integration scheme. The dependence of c_d on L is shown in Figure 1, in the left panel for $d = 4$ and in the right panel for $d = 5$. c_d turns out to be proportional to L^γ , with $\gamma \sim 3/2$, i.e. $c_d \propto \sqrt{L^3}$. This dependence is actually naïvely expected for $\text{sd}(\delta\Delta\mathcal{H})$.

Let us now turn to the other observables quoted in Table III, Table II and Table IV. First of all, in not one of the different runs with $d < 16$ a significant deviation of the plaquette expectation

value compared to the run without rounding could be detected.

However, in $\langle \exp(-\Delta\mathcal{H}) \rangle$, $\langle \Delta\mathcal{H} \rangle$ and P_{acc} we observe deviations as d is being decreased. Up to values $\text{sd}(\delta\Delta\mathcal{H}) \approx 0.1$, $\langle \exp(-\Delta\mathcal{H}) \rangle$ is compatible with one, as expected for the HMC. At the same time $\langle \Delta\mathcal{H} \rangle$ and P_{acc} are compatible within errors with the results without rounding. For $\text{sd}(\delta\Delta\mathcal{H}) \gtrsim 0.1$, we observe significant deviations in all three observables. Starting with $\text{sd}(\delta\Delta\mathcal{H}) \approx 0.1$ we also observe that the correlation

$$\rho = \text{Cor}(\Delta\mathcal{H}, \delta\Delta\mathcal{H}) \quad (30)$$

starts to increase to values around 0.5. This is an indication that the actual value of $\Delta\mathcal{H}$ is significantly influenced by the reversibility violation, thus leading to an incorrectly sampled probability distribution.

B. Dependence on the Lattice Spacing

For studying the lattice spacing dependence, we study ensembles at $\beta = 2.3$, $\beta = 2.4$ and $\beta = 2.5$. Using the length scale s_0 , we keep the physical volume approximately fixed by using $L/a = 16$ at $\beta = 2.3$, $L/a = 20$ at $\beta = 2.4$ and $L/a = 24$ at $\beta = 2.5$. The results for $\beta = 2.4$ with $L = 20$ and $\beta = 2.5$ with $L = 24$ are summarised in Table V and Table VII, respectively. Results for an additional volume for $\beta = 2.5$ with $L = 20$ are compiled in Table VI. The results for $\beta = 2.3$ have been discussed previously and can be found in Table II.

First we discuss the results for $\langle \exp(-\Delta\mathcal{H}) \rangle$ as a function of $\text{sd}(\delta\Delta\mathcal{H})$ by including all available β -values and volumes. This is shown in Figure 2 where in the left panel $\langle \exp(-\Delta\mathcal{H}) \rangle$ is plotted as a function of $\text{sd}(\delta\Delta\mathcal{H})$ with logarithmic x -axis and in the right panel $1 - \langle \exp(-\Delta\mathcal{H}) \rangle$ as a function of $\text{sd}(\delta\Delta\mathcal{H})$ with both axes logarithmic. We find that all the points fall on a universal curve within error bars. In the double logarithmic plot (right panel) it is visible that the dependence of $1 - \langle \exp(-\Delta\mathcal{H}) \rangle$ on $\text{sd}(\delta\Delta\mathcal{H})$ is like

$$1 - \langle \exp(-\Delta\mathcal{H}) \rangle \propto \text{sd}(\delta\Delta\mathcal{H})^\delta + c_3 \quad (31)$$

with some exponent δ and a constant shift c_3 . A fit to the data points with $\text{sd}(\delta\Delta\mathcal{H}) > 0.1$ reveals

$$\delta = 2.6(3)$$

and a value for c_3 significantly non-zero. The origin of the actual value of δ and in particular the non-zero shift c_3 is not clear as one would expect c_3 to be zero if reversibility was restored smoothly. At this point it is just an empirical finding.

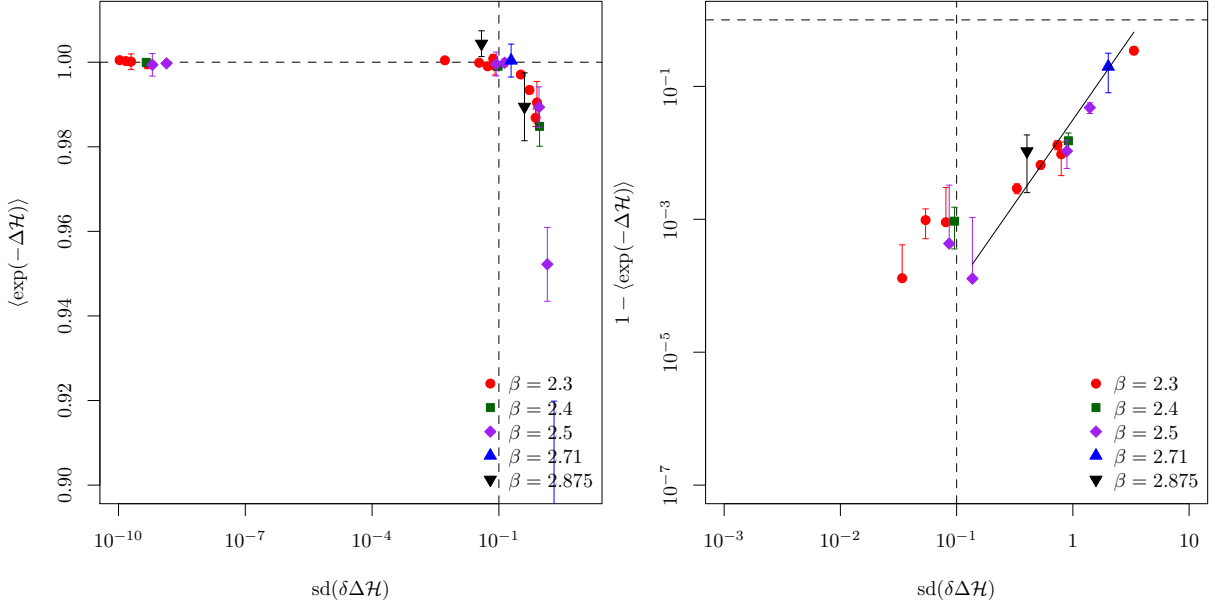


FIG. 2: Left: $\langle \exp(-\Delta\mathcal{H}) \rangle$ as a function of $sd(\delta\Delta\mathcal{H})$. Right: $1 - \langle \exp(-\Delta\mathcal{H}) \rangle$ as a function of $sd(\delta\Delta\mathcal{H})$ in a double logarithmic plot. Data for all β -values, volumes and integration schemes are shown together. In the right panel also a fit to the data is shown in the range indicated by the line.

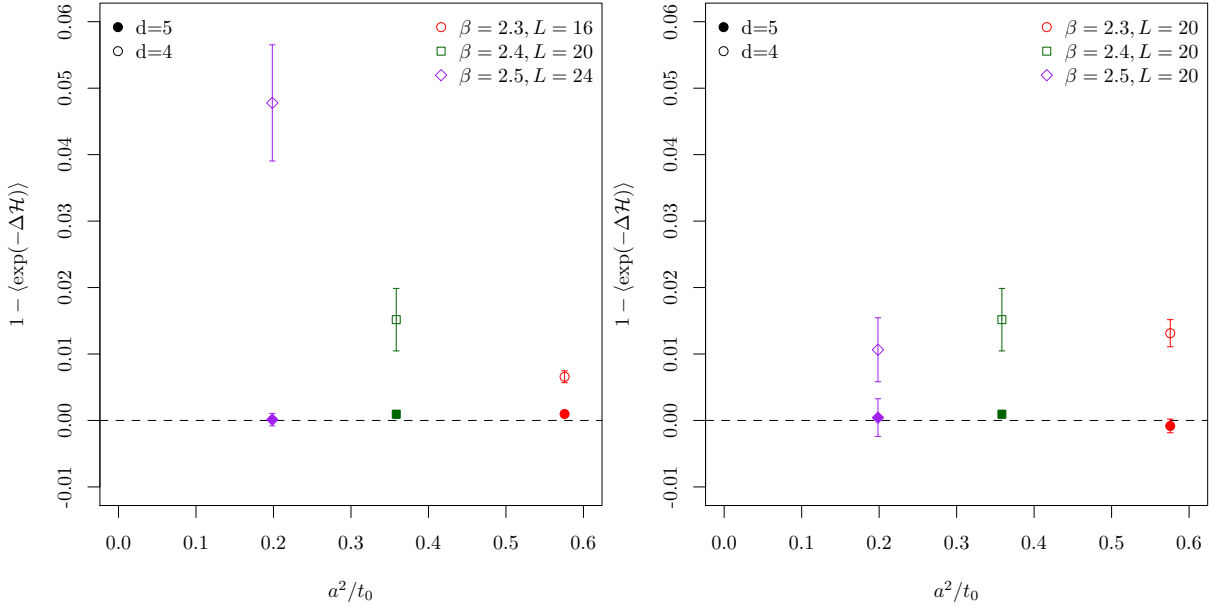


FIG. 3: $1 - \langle \exp(-\Delta\mathcal{H}) \rangle$ as a function of a^2/t_0 . Left: physical volume fixed. Right: L/a fixed.

In Figure 3 we show $1 - \langle \exp(-\Delta\mathcal{H}) \rangle$ as a function of the gradient flow scale a^2/t_0 both for $d = 4$ and $d = 5$. In the left panel we keep the physical volume, i.e. L/s_0 approximately fixed. In the right panel we keep the number of lattice points L/a fixed. In the latter case we observe

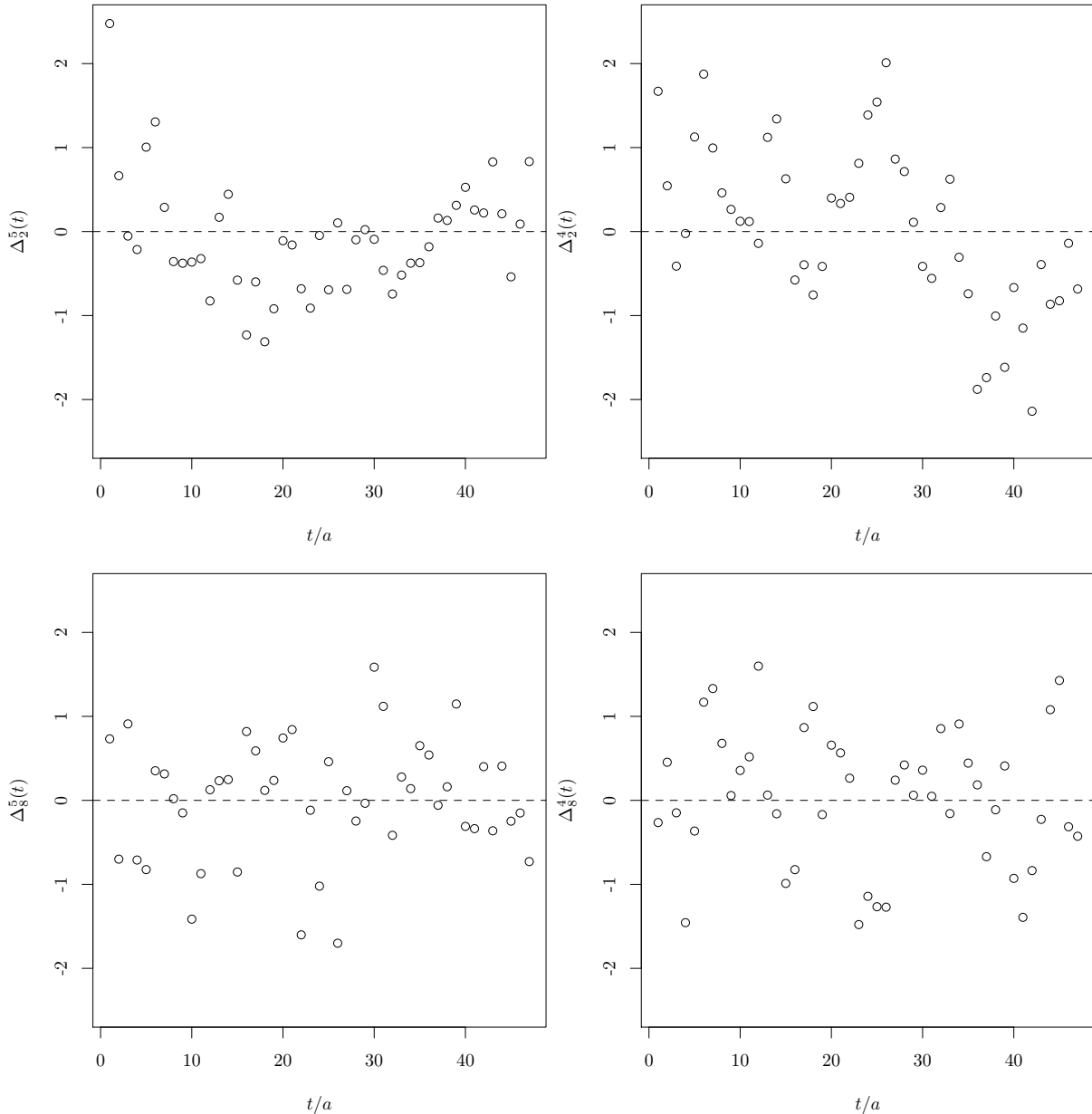


FIG. 4: Δ_r^d as a function of Euclidean time t/a measured at $\beta = 2.5$ with $L = 24$ and $T = 48$. Left: $d = 5$. Right: $d = 4$. Upper row: $r/a = 2$. Lower row: $r/a = 8$

no dependence on a^2/t_0 , neither for $d = 5$ nor for $d = 4$. For the case of fixed L/s_0 and T/s_0 we observe an increase for $d = 4$ towards smaller a^2/t_0 values.

C. Wilson Loops at $\beta = 2.5$

We have studied planar Wilson loops of fixed spatial extent r as a function of t for $\beta = 2.5$. We have computed the loops on configurations generated without deliberate rounding, with $d = 5$

and $d = 4$, see Table VII. Next we define the following normalised differences

$$\Delta_d^r(t) = \frac{C^d(t, r) - C^0(t, r)}{\sqrt{dC^d(t, r)^2 + dC^0(t, r)^2}}. \quad (32)$$

Here we denote the standard error of $C^d(t, r)$ with $dC^d(t, r)$. In Figure 4 we plot $\Delta_r^d(t)$ as a function of t/a . In the upper row we plot data for $r/a = 2$, in the lower one for $r/a = 8$. The left column corresponds to $d = 5$, the right one to $d = 4$. Note that for $r/a = 2$ the signal is lost in the noise at around $t/a = 20$ and for $r/a = 8$ around $t/a = 10$.

For $r/a = 2$, we observe a number of values of $\Delta_2^d(t)$ with modulus around 2. Still, there is no single t -value where the deviation from 0 is significant. In agreement with the results for the plaquette expectation value we, hence, find also for the exemplary Wilson loops we looked at no sign of a deviation due to reversibility violations.

V. DISCUSSION AND SUMMARY

The results presented in the last section indicate that – at least for SU(2) gauge theory – reversibility violations do not lead to deviations in the physical observables studied here. This is surprising, because for the observable $\exp(-\Delta\mathcal{H})$ with the analytically known expectation value we observe such deviations.

It turns out that good quantities to monitor reversibility are $\langle \exp(-\Delta\mathcal{H}) \rangle$ and $\text{sd}(\delta\Delta\mathcal{H})$. One observes that $\text{sd}(\delta\Delta\mathcal{H})$ is directly proportional to the rounding errors introduced deliberately in the HMC MD evolution. In the range of β -values studied here, $\langle \exp(-\Delta\mathcal{H}) \rangle$ turns out to be a universal function of $\text{sd}(\delta\Delta\mathcal{H})$, independent of integration scheme and problem size. With $\text{sd}(\delta\Delta\mathcal{H}) \lesssim 0.1$ no significant deviations of $\langle \exp(-\Delta\mathcal{H}) \rangle$ from one could be detected. For $\text{sd}(\delta\Delta\mathcal{H}) \gtrsim 0.1$ these deviations become significant and follow a power law in $\text{sd}(\delta\Delta\mathcal{H})$. It is very likely that with even larger statistical accuracy also for $\text{sd}(\delta\Delta\mathcal{H}) < 0.1$ significant deviations from one will be detectable. However, they will be tiny.

Another important observation is the fact that reversibility violations always lead to an increase in $\langle \Delta\mathcal{H} \rangle$ towards positive values. As a consequence, with too large violations the acceptance rate drops significantly. That the reversibility violations are largely responsible for the large $\Delta\mathcal{H}$ -values is indicated by the fact that for $\text{sd}(\delta\Delta\mathcal{H}) \gtrsim 0.1$ the correlation between $\Delta\mathcal{H}$ and $\delta\Delta\mathcal{H}$ becomes significant. This indicates a large influence of the reversibility violations on the accept/reject decision.

When changing β , deviations in $\langle \exp(-\Delta\mathcal{H}) \rangle$ do not depend on β if the number of lattice points

is kept constant. In turn, when the physical volume is kept constant, deviations increase towards the continuum limit. This could on the one hand be an indication that the underlying Lyapunov exponent is not varying much with β . Another possible reason could be that with trajectory lengths of $\tau = 1$ the system is still in the “random walk” regime and not yet in the regime where deviations increase exponentially. The latter interpretation is supported by the results of Ref. [10, 11].

In summary, simulations with HMC should be safe as long as $\text{sd}(\delta\Delta\mathcal{H}) < 0.1$ and correlations between $\Delta\mathcal{H}$ and $\delta\Delta\mathcal{H}$ are negligible. Those quantities are easy to monitor. In fact, $\Delta\mathcal{H}$ is available anyhow, because it is needed for the accept/reject test. $\text{sd}(\delta\Delta\mathcal{H})$ can be measured by performing reversibility tests on, say, $\mathcal{O}(100)$ trajectories. It remains to be seen whether the results found here for SU(2) gauge theory generalise to QCD with SU(3) gauge symmetry and dynamical fermions.

Acknowledgments

The author thanks K. Jansen for injecting the idea for this project a long time ago, for stimulating discussions and all his support. Thanks also to B. Kostrzewa and M. Ueding for discussions and cross-checks and to U.-G. Meißner for useful comments on the draft. The computer time for this project was made available to us in parts by the John von Neumann-Institute for Computing (NIC) on the Jureca system in Jülich. This project was funded by the DFG as a project in the Sino-German CRC110. The open source software package R [26] has been used.

Appendix A: Gradient Flow Scales

For determining the scales t_0 Eq. 27 and s_0 Eq. 28 we follow the approach presented in the original paper by Lüscher [23]. The energy density E can be defined symmetrically as the sum over the four plaquettes attached to a point x (the clover definition). This one we will denote with E_{sym} . A second possibility is to use the action Eq. 15, which we denote as E_{W} . For the exact factors see Ref. [23]. We use E_{sym} to determine the scales t_0 and s_0 , because in Ref. [23] it was found to have less lattice artefacts, and use E_{W} as a cross-check.

In Figure 5 we show $t^2E(t)$ as a function of the flow time t/a^2 for $\beta = 2.3$ (left panel) and $\beta = 2.5$ (right panel). The solid lines with error band correspond to E_{sym} and the dashed line to E_{W} . The cross indicates the determination of t_0 where $t^2E(t) = 0.1$. We observe differences between the two definitions of E which, however, decrease towards the continuum limit, as expected.

We remark here that we cannot quantitatively reproduce the results of Ref. [24] for $\beta = 2.3$.

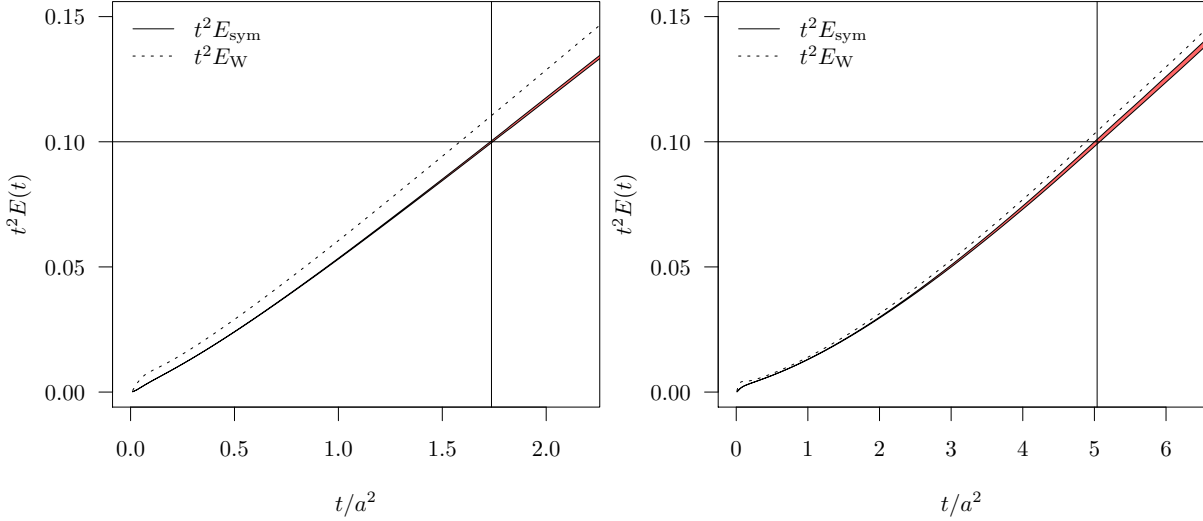


FIG. 5: Gradient flow for $\beta = 2.3$ (left) and $\beta = 2.5$ (right).

Our definition of E_{sym} differs by a factor of two to the one from Ref. [24], but this factor is not sufficient to obtain agreement. We remark that we have two independent implementations, which agree. Moreover, we have a strong test of the derivative, because it is used in the HMC as well. Apart from that the ratios of scales agree with the ones from Ref. [24], as far as this can be judged due to not exactly identical β -values.

Appendix B: Data Tables

Int	d	N_{traj}	$\langle P \rangle$	$\tau_{\text{int}}(P)$	$\langle \exp(-\Delta H) \rangle$	$\langle \Delta H \rangle$	$\text{sd}(\delta \Delta H)$	ρ	P_{acc}
OMF4	—	300009	0.60226(1)	5.4(1)	1.00048(38)	0.02191(38)	$1.0 \cdot 10^{-10}$	0.03	92
OMF4	5	555300	0.602264(4)	5.4(1)	0.99987(28)	0.02304(28)	0.03400932	0.08	91
OMF4	4	591001	0.602254(4)	5.7(1)	0.99708(49)	0.07037(48)	0.3297102	0.46	85
OMF4	3	110000	0.60227(3)	48(5)	0.655(45)	4.806(11)	3.351697	0.57	12

TABLE III: Results at $\beta = 2.3$ and $L = 12$, $T = 32$.

Int	d	N_{traj}	$\langle P \rangle$	$\tau_{\text{int}}(P)$	$\langle \exp(-\Delta H) \rangle$	$\langle \Delta H \rangle$	$\text{sd}(\delta \Delta H)$	ρ	P_{acc}
OMF4	—	170800	0.602258(4)	6.1(2)	0.9996(11)	0.1039(11)	$4.8 \cdot 10^{-10}$	-0.02	82
OMF4	5	216501	0.602261(3)	6.2(2)	1.0008(10)	0.1053(10)	0.07353326	0.08	82
OMF4	4	206501	0.602254(4)	7.3(2)	0.9869(20)	0.3276(18)	0.7368223	0.48	69

TABLE IV: Results at $\beta = 2.3$ and $L = 20$, $T = 32$.

Int	d	N_{traj}	$\langle P \rangle$	$\tau_{\text{int}}(P)$	$\langle \exp(-\Delta H) \rangle$	$\langle \Delta H \rangle$	$\text{sd}(\delta\Delta H)$	ρ	P_{acc}
OMF4	–	67401	0.630000(4)	4.7(2)	0.99996(37)	0.00551(37)	$4.5 \cdot 10^{-10}$	0.08	96
OMF4	5	50000	0.629993(5)	4.7(2)	0.99906(58)	0.01005(58)	0.0958693	0.38	94
OMF4	4	50000	0.63000(1)	7.6(5)	0.9848(47)	0.3818(39)	0.91566	0.53	66

TABLE V: Results at $\beta = 2.4$ and $L = 20$, $T = 40$.

Int	d	N_{traj}	$\langle P \rangle$	$\tau_{\text{int}}(P)$	$\langle \exp(-\Delta H) \rangle$	$\langle \Delta H \rangle$	$\text{sd}(\delta\Delta H)$	ρ	P_{acc}
OMF4	–	73900	0.651965(4)	4.9(2)	0.9994(27)	0.2197(24)	$6.3 \cdot 10^{-10}$	–0.02	74
OMF4	5	69233	0.651966(4)	4.3(2)	0.9996(28)	0.2232(25)	0.08636778	0.09	74
OMF4	4	80000	0.651962(4)	6.0(3)	0.9894(48)	0.5349(38)	0.8890045	0.48	61

TABLE VI: Results at $\beta = 2.5$ and $L = 20$, $T = 40$.

Int	d	N_{traj}	$\langle P \rangle$	$\tau_{\text{int}}(P)$	$\langle \exp(-\Delta H) \rangle$	$\langle \Delta H \rangle$	$\text{sd}(\delta\Delta H)$	ρ	P_{acc}
OMF4	–	74901	0.651967(2)	3.7(1)	0.99973(57)	0.01409(56)	$1.4 \cdot 10^{-09}$	–0.05	93
OMF4	5	46500	0.651965(3)	3.8(2)	0.99987(94)	0.02163(93)	0.136749	0.32	92
OMF4	4	45000	0.651970(4)	6.7(4)	0.9522(87)	0.8515(63)	1.398589	0.55	51

TABLE VII: Results at $\beta = 2.5$ and $L = 24$, $T = 48$.

-
- [1] S. Duane, A. D. Kennedy, B. J. Pendleton and D. Roweth, Phys. Lett. **B195**, 216 (1987).
- [2] R. Frezzotti and K. Jansen, Phys. Lett. **B402**, 328 (1997), [arXiv:hep-lat/9702016 \[hep-lat\]](#).
- [3] M. A. Clark, A. D. Kennedy and Z. Sroczynski, Nucl. Phys. Proc. Suppl. **140**, 835 (2005), [arXiv:hep-lat/0409133 \[hep-lat\]](#), [,835(2004)].
- [4] I. Montvay and E. Scholz, Phys. Lett. **B623**, 73 (2005), [arXiv:hep-lat/0506006 \[hep-lat\]](#).
- [5] M. Hasenbusch, Phys. Lett. **B519**, 177 (2001), [arXiv:hep-lat/0107019 \[hep-lat\]](#).
- [6] M. Hasenbusch and K. Jansen, Nucl. Phys. **B659**, 299 (2003), [arXiv:hep-lat/0211042 \[hep-lat\]](#).
- [7] M. Lüscher, Comput. Phys. Commun. **165**, 199 (2005), [arXiv:hep-lat/0409106 \[hep-lat\]](#).
- [8] C. Urbach, K. Jansen, A. Shindler and U. Wenger, Comput. Phys. Commun. **174**, 87 (2006), [arXiv:hep-lat/0506011 \[hep-lat\]](#).
- [9] R. G. Edwards, I. Horvath and A. D. Kennedy, Nucl. Phys. **B484**, 375 (1997), [arXiv:hep-lat/9606004 \[hep-lat\]](#).
- [10] K. Jansen and C. Liu, Nucl. Phys. **B453**, 375 (1995), [arXiv:hep-lat/9506020 \[hep-lat\]](#), [Erratum: Nucl. Phys.B459,437(1996)].
- [11] C. Liu, A. Jaster and K. Jansen, Nucl. Phys. **B524**, 603 (1998), [arXiv:hep-lat/9708017 \[hep-lat\]](#).
- [12] D. Rim, Adv. Dyn. Syst. Appl. **12**, 15 (2017), [arXiv:1505.04240 \[math.HO\]](#).
- [13] A. D. Kennedy, P. J. Silva and M. A. Clark, Phys. Rev. **D87**, 034511 (2013), [arXiv:1210.6600 \[hep-lat\]](#).
- [14] I. P. Omelyan, I. M. Mryglod and R. Folk, Comput.Phys.Commun. **151**, 272 (2003).
- [15] M. Matsumoto and T. Nishimura, ACM Trans. Model. Comput. Simul. **8**, 3 (1998), <http://doi.acm.org/10.1145/272991.272995>.
- [16] C. Urbach, HMC software for SU(2) gauge theory, <https://github.com/urbach/su2>.
- [17] B. Kostrzewa and C. Urbach, Lattice QCD analysis code, <https://github.com/urbach/hadron>.
- [18] **ALPHA** Collaboration, U. Wolff, Comput. Phys. Commun. **156**, 143 (2004), [arXiv:hep-lat/0306017 \[hep-lat\]](#), [Erratum: Comput. Phys. Commun.176,383(2007)].
- [19] M. Creutz, Phys. Rev. **D21**, 2308 (1980).
- [20] S. Perantonis, A. Huntley and C. Michael, Nucl. Phys. **B326**, 544 (1989).
- [21] A. Huntley and C. Michael, Nucl. Phys. **B270**, 123 (1986).
- [22] N. Cardoso and P. Bicudo, J. Comput. Phys. **230**, 3998 (2011), [arXiv:1010.4834 \[hep-lat\]](#).
- [23] M. Lüscher, JHEP **08**, 071 (2010), [arXiv:1006.4518 \[hep-lat\]](#), [Erratum: JHEP03,092(2014)].
- [24] B. A. Berg and D. A. Clarke, Phys. Rev. **D95**, 094508 (2017), [arXiv:1612.07347 \[hep-lat\]](#).
- [25] T. DeGrand, Phys. Rev. **D95**, 114512 (2017), [arXiv:1701.00793 \[hep-lat\]](#).
- [26] R Development Core Team, *R: A language and environment for statistical computing*, R Foundation for Statistical Computing, Vienna, Austria, 2005, ISBN 3-900051-07-0.